The Precipitation Response over the Continental United States to Cold Tropical Pacific Sea Surface Temperatures

Hailan Wang[12] and Siegfried Schubert[1]

[1]Global Modeling and Assimilation Office, NASA Goddard Space Flight Center

[2]Science Systems and Applications, Inc.

Submitted to *Journal of Climate*

July 29, 2013

ABSTRACT

The dominant pattern of annual mean SST variability in the Pacific (in its cold phase) produces pronounced precipitation deficits over the continental United States (U.S.) throughout the annual cycle. This study investigates the physical and dynamical processes through which the cold Pacific pattern affects the U.S. precipitation, particularly the causes for the peak dry impacts in fall, as well as the nature of the differences between the summer and fall responses.

Results, based on observations and reanalyses, show that the peak precipitation deficit over the U.S. during fall is primarily due to reduced atmospheric moisture transport from the Gulf of Mexico into the central and eastern U.S., and secondarily due to a reduction in local evaporation from land-atmosphere feedback. The former is associated with a strong and systematic low-level northeasterly flow anomaly over the southeastern U.S. that counteracts the northwest branch of the climatological flow associated with the north Atlantic subtropical high. The above northeasterly anomaly is maintained by both diabatic heating anomalies in the nearby Intra-American Seas and diabatic cooling anomalies in the tropical Pacific. In contrast, the modest summertime precipitation deficit over the U.S. is mainly the result of local land-atmosphere feedback; the rather weak and disorganized atmospheric circulation anomalies over and to the south of the U.S. make little contribution. An evaluation of NSIPP-1 AGCM simulations shows it to be deficient in simulating the warm season tropical convection responses over the Intra-American Seas to the cold Pacific pattern and thereby the precipitation responses over the U.S., a problem that appears to be common to many AGCMs.

38

1. Introduction

39

40 The leading annual mean Sea Surface Temperature (SST) patterns, obtained as the three leading
41 Rotated Empirical Orthogonal Functions (REOFs) of annual mean SST over the period 1901-
42 2004, consist of a global trend pattern, a Pacific pattern, and an Atlantic pattern (Schubert et al.
43 2009). Among these, the Pacific pattern (Figure 1) has the most pronounced influence over the
44 U.S. throughout the annual cycle, with the other two SST patterns playing secondary roles (e.g.
45 Mo et al. 2009; Schubert et al. 2009). The Pacific pattern contains signals from both the El
46 Niño–Southern Oscillation *(*ENSO) and Pacific Decadal Variability (PDV); its cold phase is
47 characterized by cold SST anomalies along the central and eastern tropical Pacific, and warm
48 SST anomalies along 40ºN in the north Pacific. The associated Principal Component (PC) shows
49 the ENSO signals superimposed upon a negative PDV prior to mid-1920s, during 1947-1976,
50 and after the late 1990s, and a positive PDV during 1925-1946 and from 1977 to the mid-1990s.

51 Figure 2 shows that the cold (negative) phase of the Pacific pattern is generally associated with
52 precipitation deficits over the U.S.[1] throughout the annual cycle. Such precipitation deficits are
53 more prominent during the transition seasons compared with winter and summer. In particular,
54 the peak deficits occur during fall. Figure 2 also shows that, during winter, the precipitation
55 anomalies resemble those associated with La Nina, with deficits along the southeastern and
56 southwestern U.S., and positive anomalies along the Ohio Valley and the northwestern U.S. The
57 springtime precipitation anomalies show distinct dry anomalies over the central U.S. as well as

[1] The observed precipitation anomalies over the U.S. associated with the cold Pacific SST pattern in Figure 2 is obtained by compositing the HadCRU TS3.0 precipitation data (Mitchell and Jones 2005) for years that exceed one standard deviation of the PC of the cold Pacific pattern over the period 1901-2004.

along the southeastern and southwestern coasts of the U.S., with some wet anomalies further north. During summer, the dry anomalies mainly occur over the Great Plains with moderate amplitude; there is an increase in precipitation over the southeastern U.S. except for central and southern Florida where there are strong precipitation decreases. During fall, there are pronounced deficits over the entire central U.S., with precipitation increases occurring only along the eastern coastal states. The strong precipitation deficit during fall stands out among the four seasons.

While the effects of Pacific SST over the U.S. during winter and summer have been extensively studied using observations (e.g., Trenberth et al 1998; Ting and Wang 1998; Dai 2012), the overall seasonality of the effects, particularly the peak in fall, has received far less attention. Past observational studies that investigate the U.S. precipitation during fall mainly focused on its trend and leading variability. The largest precipitation trend over the U.S. during fall has been associated with more frequent rain occurrence in that season (Small and Islam 2008; 2009). The leading mode of fall precipitation variability over the North America has been linked to a hemispheric-scale circulation pattern that stretches from the western Pacific to the north Atlantic (Small et al. 2010). The nature of the relatively large fall precipitation anomalies associated with the cold Pacific pattern, however, has not been addressed in any previous studies.

The seasonal effects of the cold Pacific SST over the U.S. have been investigated using GCM simulations (e.g. Wang et al 2010), with the caution that model-based findings are subject to possible model deficiencies. Using National Aeronautics and Space Administration (NASA) Seasonal to Inter-annual Prediction Project (NSIPP-1) Atmospheric GCM (AGCM) simulations, Wang et al (2010) has investigated the physical mechanisms by which the cold Pacific pattern impacts U.S. precipitation throughout the annual cycle. Compared with the observations (Figure

2), which have the peak deficit in fall, the model shows the peak response in summer (Figure 2, Wang et al 2010). The strong summertime precipitation deficit in the model is caused by reduced moisture transport into the central U.S. associated with an anomalous low-level cyclonic flow over the Gulf of Mexico, and further amplification by strong soil moisture feedback over the U.S. The circulation anomalies are maintained by diabatic heating anomalies over the Gulf of Mexico as a secondary response to circulation anomalies forced from the tropical Pacific.

In light of the above differences in the U.S. precipitation responses found in the model (Wang et al 2010) and observations (Figure 2), this study carries out a more in-depth observationally-based analysis of the physical and dynamical processes through which the cold Pacific pattern affects the U.S. precipitation throughout the annual cycle, with the focus on the peak deficit during fall. The results are compared with those from the NASA NSIPP-1 AGCM simulations (Wang et al. 2010), with the aim of identifying potential model deficiencies in representing the effects of the cold Pacific pattern over the U.S.

The paper is organized as follows. Section 2 describes the data and methods used in this study. Section 3 investigates the physical processes by which the cold Pacific SST pattern affects the U.S. precipitation, particularly during fall, and examines the dependence of the results on the observational (including reanalysis) data used. In addition, the key processes revealed from the reanalyses are compared with those found to be operating in the NSIPP-1 AGCM simulations. The summary and conclusions are given in Section 4.

2. Data and Methods

2.1. Observations, reanalyses and AGCM simulations

101 The precipitation observations used in this study are the HadCRU TS3.0 (Mitchell and Jones
102 2005) monthly data. These data have fine spatial resolution (0.5 latitude by 0.5 longitude), and
103 are available for a sufficiently long time period (January 1901 through June 2006) to
104 accommodate our composite analysis. While the quality of these data is limited by the sparse
105 coverage of the station observations over some regions of the world especially in the earlier time
106 periods, it is reliable over the U.S. because of the relatively dense observational network
107 throughout the entire time period.

108 In order to investigate the physical and dynamical processes by which the cold Pacific pattern
109 affects the U.S., we use the Modern-Era Retrospective Analysis for Research and Applications
110 (MERRA)-Scout reanalysis data (Wang et al. 2009) produced at the NASA Global Modeling and
111 Assimilation Office (GMAO). The Scout reanalysis was generated using the same observations
112 and data assimilation system as MERRA (Rienecker et al. 2011), with the primary difference
113 being the coarser (2° latitude by 2.5°longitude) spatial resolution and that it dates back to the
114 year 1948[2].

115 To investigate the dependence of our results on the specific reanalysis used, we analyze
116 atmospheric circulation fields from two other reanalysis data sets that are available over the
117 period 1948-present, i.e., the National Center for Environmental Prediction (NCEP)/National
118 Center for Atmospheric Research (NCAR) reanalysis (Kalnay et al. 1996) and the Twentieth
119 Century reanalysis (Compo et al. 2011). The NCEP/NCAR reanalysis and the 20th Century
120 reanalysis are based on data assimilation systems and input observations considerably different
121 from that of the Scout reanalysis. The NCEP/NCAR reanalysis, one of the so-called first

[2] The Scout reanalysis was initially intended as a coarse resolution precursor to MERRA (available from 1979-present) to allow addressing (scouting for) potential technical issues with the input observations prior to the start of MERRA, but was later extended back to 1948 to provide a resource for addressing decadal variability.

generation reanalyses, is described in Kalnay et al. (1996), and has been widely used and shown to be valuable for a wide range of climate research. The 20th Century reanalysis (Comp et al. 2011) assimilates surface pressure observations only. It uses an Ensemble Kalman Filter data assimilation method with background 'first guess' fields supplied by an ensemble of forecasts from a global numerical weather prediction model. The above three reanalyses have their advantages and disadvantages. The Scout reanalysis and the NCEP/NCAR reanalysis assimilate a wide range of input observations. Thus, both of them are likely to be influenced by changes in the observing system. In contrast, by assimilating surface pressure observations only, the 20th Century reanalysis is less impacted by input observation changes; on the other hand, it may be more problematic in representing atmospheric circulation and moisture, as the observations of these fields are not assimilated. In this study, we examine the atmospheric circulation in all three reanalyses, and consider features common to all of them as more reliable and representative of nature.

The NSIPP-1 AGCM simulations consist of an ensemble of fourteen Atmospheric Modeling Inter-comparison Project (AMIP) type simulations made for the period 1902-2004, as well as, idealized AGCM experiments performed for the U.S. Climate Variability and Predictability (CLIVAR) drought project (Schubert et al. 2009). The latter consists of a control run forced with a seasonally varying SST climatology, and an anomaly run forced with the cold Pacific pattern (Figure 1) superimposed onto the seasonally varying SST climatology: both are 99 years long. The model response to the cold Pacific in the idealized AGCM experiment is obtained as the mean difference between the control run and the anomaly cold Pacific runs averaged over the last 80 years. For the above experiments, the NSIPP-1 AGCM is run with a horizontal resolution of 3 degrees latitude/longitude. Details of the NSIPP-1 model formulation and its climate are

described in Bacmeister et al. (2000). The seasonal predictability of the model is described in Pegion et al. (2000) for boreal winter, and in Schubert et al. (2002) for boreal summer. The physical mechanisms through which the cold Pacific pattern affects the U.S. precipitation in the NSIPP-1 AGCM are investigated in Wang et al. (2010).

2.2. Analysis methods

Our investigation of the impacts of the cold Pacific pattern includes the computation and analysis of atmospheric moisture budgets and various diagnostics using stationary wave modeling. In these analyses, anomalies associated with the cold (negative) phase of the Pacific pattern are obtained as a composite average of values for years during which the PC of the Pacific pattern is less than minus one standard deviation over the period that both the PC and the anomaly fields are available. We note that varying the standard deviation criteria from 0.8 to 1.2 does not lead to any notable differences (not shown).

The atmospheric moisture budget analysis is used to examine how the precipitation anomalies over the U.S. are balanced by evaporation anomalies and changes in atmospheric transient and stationary moisture flux convergences. The changes in stationary moisture flux convergences are further decomposed into those due to changes in atmospheric moisture and those due to changes in atmospheric circulation. Wang et al. (2010) provides more details of the atmospheric moisture budget analysis.

Atmospheric moisture budgets based on reanalyses have proven useful for investigating key processes affecting U.S. precipitation (e.g. Mo and Higgins 1996; Mo et al 2005). Since atmospheric wind and specific humidity fields in reanalysis are subjected to analysis adjustment

terms, the atmospheric moisture budget using reanalysis is not strictly closed. Here we do not intend to pursue a quantitatively closed budget, but rather to explore the main physical processes for the precipitation anomalies over the U.S. Among the variables needed for the atmospheric moisture budget in the Scout reanalysis, atmospheric wind fields are strongly constrained by the observations while specific humidity is potentially more strongly influenced by any bias in the assimilating model; precipitation and evaporation are not assimilated and are derived solely from the model forced by the data assimilation. The rather dense observational network over the U.S. and nearby area throughout the period 1948-present, including the dense conventional station observations during the pre-satellite era, provides us with confidence in using the Scout reanalysis for the atmospheric moisture budget analysis over these regions.

Since the changes in stationary moisture flux convergences due to changes in atmospheric circulation often play an important role in explaining the precipitation anomalies, the maintenance of the atmospheric circulation anomalies is further investigated using a diagnostic stationary wave modeling approach. The stationary wave model used in this study is nonlinear, time-dependent, and based on three-dimensional primitive equations. It has rhomboidal wavenumber 30 truncation in the horizontal, and 14 unequally spaced sigma levels in the vertical. This model has been shown to be a valuable tool to diagnose the relative roles of regional forcing anomalies for atmospheric circulation anomalies on various time scales (e.g. Lau et al. 2004; Schubert et al. 2011). Ting and Yu (1998) and Held et al. (2002) provide details of the stationary wave model.

In the stationary wave modeling experiments performed for this study, the basic state consists of the three-dimensional (3-D) climatological seasonal mean zonal and meridional wind, air

188 temperature and two-dimensional (2-D) surface pressure. The climatology is for the period 1948-
189 2004, when both the PC of the Pacific pattern and the Scout reanalysis are available. The
190 stationary wave forcing consists of 3-D diabatic heating anomalies, and anomalies in the
191 vorticity, divergence and thermal transient flux convergences. Following Wang and Ting (1999),
192 the monthly diabatic heating in the Scout reanalysis is derived as a residual based on the
193 thermodynamic equation in pressure coordinates; the monthly transient forcings are obtained by
194 computing the major terms in the vorticity, divergence and temperature equations in pressure
195 coordinates. The above stationary wave forcings are then linearly interpolated onto the spatial
196 grids of the stationary wave model. The seasonal mean stationary wave forcing anomalies
197 associated with the cold (negative) Pacific pattern are obtained as a composite average over those
198 years (during 1948-2004) for which the PC of the Pacific pattern is less than minus one standard
199 deviation (Figure 1).

200 **3. Results**

201 In this Section, the physical and dynamical processes by which the cold Pacific SST pattern
202 affects precipitation over the U.S., particularly during fall, are investigated using the Scout
203 reanalysis. The dependence of our results on the Scout reanalysis is investigated by analyzing
204 atmospheric circulation anomalies in two other reanalyses. Lastly, the NSIPP-1 AGCM
205 simulation of the seasonal effects of the cold Pacific pattern over the U.S. is evaluated based on a
206 comparison with observations and the reanalyses.

207 *3.1. Seasonality of the effects of the cold Pacific SST pattern over the U.S.*

208 Figure 3 shows seasonal mean precipitation anomalies over the U.S. associated with the cold
209 Pacific pattern based on the Scout reanalysis for the period 1948-2004 (Figure 1). Despite
210 relatively coarse resolution and not assimilating observed precipitation, the Scout reanalysis
211 (Figure 3) captures the majority of the observed features for all four seasons fairly well (cf.
212 Figure 2)[3]. Consistent with the HadCRU TS3.0 results, during winter, the Scout reanalysis shows
213 precipitation deficits over southeastern and southwestern U.S., and precipitation increases along
214 the Ohio Valley and over northwestern U.S.. Spring exhibits dry responses over the central U.S.
215 with wet responses further north. The summertime precipitation anomalies show precipitation
216 reductions in the central U.S. and southern coastal U.S., and increases over states along the
217 northwestern U.S.-Canadian border. The fall season has the largest precipitation deficits
218 spanning the entire central U.S., with moderate precipitation increases over the eastern coastal
219 states. Given the above good agreement between the Scout reanalysis and the HadCRU
220 observations, we next use the Scout reanalysis to examine the atmospheric moisture budget over
221 the U.S. and nearby regions.

222 *3.2. Physical and dynamical processes from Scout reanalysis*

223 *3.2.1. Atmospheric moisture budget analysis*

224 Figure 4 shows the atmospheric moisture budget for all four seasons based on the Scout
225 reanalysis. During winter (Figure 4a), the precipitation deficits over the southeastern and
226 southwestern U.S. are mainly tied to anomalies in transient moisture flux convergences. This is
227 consistent with many previous observational studies (e.g. Trenberth et al 1998). During spring
228 (Figure 4b), the precipitation deficits over the central U.S. and eastern coastal U.S. are affected

[3] Note the composite results for HadCRU TS3.0 over the period 1948-2004 do not differ notably from those over the period 1901-2004 shown in Figure 2.

by all the budget terms. The deficit over the central U.S. is maintained by a reduction in evaporation and weaker transient moisture flux convergences. The deficit over the eastern U.S. is mainly due to weaker stationary moisture flux convergences that are associated with a high anomaly centered over the Gulf of Mexico: the southerly wind anomaly to its west brings moisture into U.S. leading to a precipitation increase over the central U.S., while the westerlies to its north contribute to dry conditions over the eastern U.S. During summer (Figure 4c), the moderate precipitation deficits over the central and eastern U.S. are mainly balanced by reductions in evaporation, a reflection of local land-atmosphere feedback. The changes in both the transient and stationary moisture flux convergences are weak. In particular, weak and disorganized low-level flow anomalies produce vertically integrated stationary moisture flux convergence anomalies that contribute little to the precipitation deficit over the U.S.. The negative anomaly in atmospheric moisture only contributes to weaker stationary moisture flux convergence over part of Midwestern U.S..

During fall (Figure 4d), the relatively large precipitation deficits over the majority of the U.S. are primarily linked to changes in stationary moisture flux convergences due to changes in the low-level atmospheric circulation, and secondly the result of a reduction in local evaporation from land-atmosphere feedback. The low-level atmospheric circulation anomalies are characterized by a strong and systematic northeasterly wind anomaly spanning the southeastern U.S., the northwestern branch of a broad cyclonic flow anomaly over the Northern Hemisphere (NH) Atlantic, and the eastern and southeastern U.S.. Counteracting the climatological southwesterlies to the northwest of the climatological North Atlantic subtropical high, the northeasterly flow anomaly weakens the climatological atmospheric moisture transport from the Gulf of Mexico into the U.S., leading to dry anomalies over the U.S..

252 *3.2.2. Stationary wave modeling diagnosis*

253 Given the importance of the low-level northeasterly flow anomaly over the southeastern U.S. for
254 maintaining the precipitation deficit during fall, we next investigate its maintenance using a
255 stationary wave model (Figure 5). When forced with the sum of diabatic heating and transient
256 flux convergence anomalies, the stationary wave model (Figure 5b) reproduces the Scout
257 reanalysis (Figures 5a) fairly well. The low-level cyclonic flow anomaly centered over the Gulf
258 of Mexico and the Caribbean Sea that includes the northeasterly flow anomaly at its
259 northwestern branch, the key feature of interest, is well captured by the stationary wave model.
260 Other major features, including the low anomaly over central South America, a pair of cyclonic
261 flow anomalies straddling the equator over the Indian Ocean (not shown), and the pair of
262 anticyclonic flow anomalies over the Pacific Ocean, are all very well simulated by the stationary
263 wave model. Such good agreement not only suggests that the Scout reanalysis data are
264 dynamically consistent with the stationary wave model, but also shows the capability of the
265 stationary wave model in reproducing the reanalysis atmospheric circulation features. We next
266 further decompose the total response into the responses to various regional stationary wave
267 forcing anomalies. The comparison of the stationary wave model response to total forcing
268 (Figure 5b) with the responses to diabatic heating (Figure 5c) and transient forcing (Figure 5d)
269 anomalies shows the importance of the diabatic heating anomalies in explaining the majority of
270 the low-level atmospheric circulation features in the NH Pacific and over North America; the
271 transient forcing anomaly plays a negligible role over the southeastern U.S. and the subtropical
272 north Atlantic. The stationary wave model response to global diabatic heating anomalies (Figure
273 5c) is further decomposed into those due to heating in the tropical Pacific (west of 250ºE)
274 (Figure 5e) and nearby heating over the tropical American regions (east of 250ºE) (Figure 5f),

the latter of which is further separated into the diabatic cooling anomalies over the eastern tropical Pacific (Figure 5g) and the heating anomalies over the Intra-American Seas (Figure 5h). The results show that the low-level cyclonic flow anomaly over the Gulf of Mexico is forced by diabatic heating anomalies in both nearby areas and in the tropical Pacific. Among the nearby diabatic heating and cooling anomalies, the positive heating anomaly over the Intra-American Seas plays an important role in maintaining the low-level cyclonic anomaly over the Gulf of Mexico, whereas the cooling anomaly over the eastern tropical Pacific produces a high anomaly over the NH tropical and subtropical Pacific which partly offsets the low anomaly due to the heating over Intra-American Sea regions thereby helping to shape the northeasterly flow anomaly over the southeastern U.S.

In contrast to fall, during which the low-level atmospheric circulation anomalies strongly contribute to the precipitation deficits over the U.S., summer shows little contribution from atmospheric circulation anomalies, as they are quite weak over the U.S. and oceanic regions further south (Figure 6a). When forced with the sum of global stationary wave forcing anomalies (Figure 6b), the stationary wave model reproduces the summertime low-level atmospheric circulation anomalies in the Scout reanalysis, including the weak and disorganized flow anomalies over and to the south of the U.S. Further decomposition of the total response (Figure 6b) into those due to individual stationary wave forcing anomalies shows the predominant role of global diabatic heating (Figure 6c). The separation of the global heating anomalies (Figure 6c) into those in the remote tropical Pacific (Figure 6e) and those in the Intra-American Sea regions (Figure 6f), shows that neither of them exerts notable circulation anomalies over the U.S. and regions to its south.

297 An additional set of stationary wave modeling experiments that use mixed combinations of basic
298 state and stationary wave forcing anomalies for summer and fall (not shown) indicate that, the
299 strong low-level atmospheric circulation anomalies during fall are mainly the result of the
300 particular stationary wave *forcing* anomalies during that season: the seasonal change in the *basic*
301 *state* from summer to fall does not appear to be important in explaining the difference between
302 summer and fall.

303 *3.3. Dependence of the results on the reanalysis*

304 The mechanisms by which the cold Pacific pattern affects the U.S. revealed in Section 3.2 are
305 based on the Scout reanalysis over the period 1948-2004. Since the quality of any reanalysis
306 over the pre-satellite time period (1948-1978) is likely to be impacted by model bias, especially
307 over regions where conventional data are limited, we next examine two other reanalyses that are
308 available over the period 1948-2004 (the NCEP/NCAR reanalysis and the 20th Century
309 reanalysis). Given that these three reanalyses are generated using different data assimilation
310 methods and models, we hypothesize that if the atmospheric circulation features of interest are
311 common to all three reanalyses, then they are more likely to be realistic.

312 Figure 7 compares the low-level atmospheric circulation anomalies for both summer and fall
313 computed from the three reanalyses. During summer, consistent with the Scout reanalysis, the
314 other two reanalyses also show rather weak low-level flow anomalies over the U.S., the Gulf of
315 Mexico and nearby regions, in support of the result of a weak contribution from changes in
316 atmospheric circulations for precipitation changes during that season. The three reanalyses are
317 consistent with each other over other regions as well, including the strong equatorial westerly
318 anomalies over the tropical Pacific, a high anomaly over the north Pacific, and a localized low

anomaly off the northwest coast of North America. During fall, the NCEP/NCAR and the 20th Century reanalyses are remarkably consistent with the Scout reanalysis in that they also show strong easterly flow over the North Atlantic, and northeasterly flow over the southeastern U.S. which further turns south into the Gulf of Mexico and then eastward over the Caribbean Sea. All three reanalyses also agree with each other reasonably well over other regions, including the high anomaly over the North Pacific, and the strong westerly anomaly along the equatorial Pacific associated with the cold Pacific pattern. The good agreement between the three reanalyses supports our basic result that during fall the cold Pacific pattern affects the U.S. precipitation through the strong northeasterly flow anomaly over the southeastern U.S.

Two additional sets of stationary wave modeling experiments are performed to examine the role of diabatic heating anomalies in the NCEP/NCAR and 20th Century reanalyses in producing the northeasterly anomaly over the southeastern U.S. during fall. In this case, for simplicity the diabatic heating anomalies are constructed using the reanalysis precipitation[4]. The use of reanalysis precipitation to estimate the diabatic heating is justified by the dominance of latent heat release in the total diabatic heating in the tropics and subtropics, Comparing Figures 8 and 5, we see that there is indeed good agreement between the precipitation and heating anomalies in the tropics and subtropics for the Scout reanalysis. We note our intention here is to confirm the importance of diabatic heating for maintaining the atmospheric circulation over the southeastern U.S. in the other two reanalyses, rather than to repeat the more detailed analysis done for the Scout reanalysis, as this is rather expensive computationally.

[4] The latent heating anomalies for the NCEP/NCAR reanalysis and the 20th Century reanalysis are estimated from the precipitation anomalies using the equation for latent heat release, and assuming a vertical profile with the maximum at $\sigma = 0.5$ that is characteristic of the vertical distribution of diabatic heating anomalies in the tropics and subtropics.

Figure 8 compares the three reanalyses in the tropical and subtropical precipitation anomalies as proxy for diabatic heating anomalies. During summer and fall, the reanalyses agree with each other in the large-scale features of the precipitation responses. These include cold ENSO-like precipitation responses in the tropical Pacific, and precipitation increases over tropical America associated with anomalous ascent induced by the cold Pacific SST anomaly. There are however notable differences in regional details. In the tropical Pacific, compared with the Scout reanalysis, the NCEP/NCAR reanalysis shows a noisier spatial distribution, and the 20th Century has stronger precipitation anomalies. Over the Intra-American Sea regions, the Scout reanalysis has positive precipitation anomalies over the Amazon, and the oceanic regions off the west coast of Mexico and the tropical Atlantic Ocean; the NCEP/NCAR reanalysis has positive precipitation anomalies over the Caribbean Sea, and the western tropical Atlantic and northeastern Brazil, whereas the 20th Century reanalysis has patched positive precipitation anomalies over and to the west of Mexico, western and eastern tropical Atlantic and eastern South America. Given the above similarities and differences in the precipitation anomalies, we next use the stationary wave model to investigate whether the northeasterly flow anomaly over the southeastern U.S., the feature that is present in all three reanalyses, also has similar maintenance characteristics in the reanalyses.

Figure 9 shows that, even with such simply constructed latent heating anomalies, the large-scale atmospheric circulation features in the tropics and subtropics, including the low-level cyclonic flow anomaly over the NH western tropical Atlantic, are well captured in both reanalyses. The stationary wave response to the total heating anomalies is further decomposed into those in the remote tropical Pacific (west of 250ºE) and those over the U.S. and the oceanic regions further south (east of 250ºE). Figure 9 shows that the low anomaly over the NH western tropical Atlantic

362 in the NCEP/NCAR reanalysis is mainly due to heating anomalies over the Intra-American Seas,
363 whereas the low anomaly in the 20th Century reanalysis is mostly forced by heating anomalies in
364 the tropical Pacific. The different contribution from heating anomalies in remote and nearby
365 regions in these reanalyses is not surprising. When performing composite analysis over the
366 period 1948-2004, a number of the cold Pacific years fall in the pre-satellite time period (1948-
367 1978). The precipitation and diabatic heating composites in the tropical and subtropical oceans in
368 the reanalyses therefore are likely affected by the poorer quality of the data during that time
369 period, as more limited observational coverage results in greater model dependencies.
370 Nevertheless, the above results suggest that the northeasterly flow anomaly over the southeastern
371 U.S during fall is constructively maintained by the cooling anomalies in the tropical Pacific and
372 heating anomalies over the Intra-American Sea regions, though their relative importance is
373 unclear.

374 *3.4. The NSIPP-1 AGCM simulations*

375 AGCM simulations have proven to be a powerful tool for investigating the mechanisms
376 responsible for U.S. precipitation variations (e.g. Schubert et al 2004; Seager et al 2005; Wang et
377 al 2010). The impacts of the leading SST patterns on U.S. hydroclimate have been extensively
378 investigated in a series of studies as part of a USCLIVAR Drought Working Group project
379 (Schubert et al. 2009). Our results based on reanalysis data (Sections 3.2 and 3.3) suggest that,
380 in order for a model to correctly simulate the warm season precipitation response over the U.S. to
381 SST changes in the tropical Pacific, it must correctly simulate the tropical convection response
382 over both the tropical Pacific and the Intra-American Sea regions. It is of practical interest to
383 examine how well AGCMs represent the key processes revealed in Section 3.2, and identify

potential model deficiencies so as to improve these models. Here we focus on the NSIPP-1 AGCM (one of the models used in the US CLIVAR project), since the physical mechanisms through which the leading SST patterns affect U.S. precipitation have already been thoroughly investigated for this model in Wang et al (2010).

We begin by comparing the atmospheric moisture budget and stationary wave modeling diagnosis results from the NSIPP-1 AGCM produced in Wang et al (2010) to the results in Section 3.2. When comparing Figure 10 with Figure 4, it should be kept in mind that the results for the NSIPP-1 AGCM are based on an idealized AGCM run forced with the cold Pacific pattern with a weight of two standard deviations, whereas the composite results from the reanalysis (Figure 4) are based on all the time periods for which the cold Pacific pattern exhibits amplitudes greater than one standard deviation. Additionally, the effects of any seasonal variations in the SST anomalies associated with the cold Pacific SST pattern are not included in the idealized AGCM run. Such effects however do not appear to be important, as the precipitation responses from the idealized AGCM runs exhibit strong similarity to the composite results from the AMIP simulations, particularly in spatial pattern (not shown). The strong similarity also suggests that SST anomalies in other oceanic basins that are generated in response to the cold Pacific SST through atmospheric tele-connection and air-sea interaction only play secondary roles.

The comparison between the NSIPP-1 AGCM (Figure 10a) and the Scout reanalysis (Figure 4a) precipitation anomalies shows good agreement during winter. The NSIPP-1 AGCM response to the cold Pacific pattern is a precipitation deficit over the southeastern and southwestern U.S., and a precipitation increase over the northwestern U.S.. Such responses are mainly associated with

406 changes in transient moisture flux convergences. During spring, while the large-scale features in
407 the NSIPP-1 AGCM are generally consistent with those in the Scout reanalysis, the NSIPP-1
408 AGCM (bottom panel of Figure 10b) shows a high anomaly that is zonally too extensive over the
409 southern U.S., the northwesterly flow to its northeast leads to too strong a dry response over the
410 eastern and southeastern U.S. Summer shows the most distinct difference between the NSIPP-1
411 AGCM and the Scout reanalysis. The moderate summertime precipitation deficit responses in the
412 Scout reanalysis are mainly maintained by a reduction in evaporation. In contrast, the rather
413 strong precipitation deficits over the central U.S. in the NSIPP-1 AGCM simulations are
414 maintained by not only an evaporation reduction from local atmosphere-land feedback, but also
415 by reduced atmospheric moisture transport associated with a strong low-level cyclonic flow
416 anomaly centered over the Gulf of Mexico which is itself maintained by the strong local heating
417 anomaly (Wang et al 2010). The above differences between the NSIPP-1 AGCM and the Scout
418 reanalysis partly originate from their heating differences over Intra-American Seas, and partly
419 from the model overestimation of observed land-atmosphere coupling strength during summer
420 (Koster et al. 2003).

421 During fall, the NSIPP-1 AGCM generally agrees with the Scout reanalysis in the precipitation
422 deficit responses over the central U.S., except that the deficits in the model simulations are
423 somewhat weaker and located further west. While in both the NSIPP-1 AGCM and the Scout
424 reanalysis, the precipitation deficits are primarily associated with changes in evaporation and
425 stationary moisture flux convergences due to changes in low-level atmospheric circulations, the
426 low-level circulation pattern and maintenance is different. In contrast with the Scout reanalysis
427 in which the low-level low anomaly resides over the NH western tropical Atlantic and is
428 maintained by both cooling anomalies in the tropical Pacific and heating anomaly over the Intra-

American Seas, the NSIPP-1 AGCM has its low-level cyclonic flow anomaly centered over the Gulf of Mexico, and it is mainly forced by the strong and localized heating anomalies there (Wang et al 2010). The differences between the NSIPP-1 AGCM and the Scout reanalysis during fall again result from the differences in the heating in the Intra-American Seas.

The above comparison between the NSIPP-1 AGCM and the Scout reanalysis suggests that the NSIPP-1 AGCM is deficient in simulating the remote warm season tropical convective responses over the Intra-American Sea to SST changes in the tropical Pacific. Different from the reanalyses (Figure 8), the NSIPP-1 AGCM places the enhanced precipitation and diabatic heating anomalies over the Gulf of Mexico during warm seasons (Figure 11). In fact, Wang et al. (2010) has shown that all the AGCMs participating in the USCLIVAR drought working group project exhibit rather large uncertainty (differences) in representing tropical convection responses in the Intra-American Sea region during the warm seasons.

4. Summary and Conclusions

The leading pattern of annual mean SST variability in the Pacific (in its cold phase) produces pronounced precipitation deficits over the U.S. throughout the annual cycle, with the peak reached in fall. Using observations and the MERRA-Scout reanalysis, this study investigated the physical and dynamical processes through which the cold Pacific pattern affects the precipitation over the U.S., particularly the causes for the peak dry impacts in fall, and how that differs from the response during the summer. In addition, this study evaluated the quality of the NASA NSIPP-1 AGCM in simulating the effect of the cold Pacific SST on U.S. precipitation.

The results show that the peak precipitation deficit over the U.S. during fall is primarily due to a reduction in atmospheric moisture flux from the Gulf of Mexico into the central and eastern U.S.,

and secondly due to a reduction in evaporation from local land-atmosphere feedback. The former is associated with a strong and systematic low-level northeasterly flow anomaly over the southeastern U.S. that counteracts the climatological low-level flow associated with the northwest branch of the north Atlantic subtropical high. The diagnosis of the results using a stationary wave model shows that the northeasterly anomaly is constructively maintained by diabatic heating anomalies in the nearby Intra-American Sea regions and diabatic cooling anomalies in the remote tropical Pacific. By comparison, the moderate summertime precipitation deficit response over the U.S. is mainly the result of local land-atmosphere feedback. The negative anomaly in atmospheric moisture only contributes to weaker stationary moisture flux convergence over Midwestern U.S.. The rather weak and disorganized atmospheric circulation anomalies over and to the south of the U.S. lead to only small stationary moisture flux convergence changes over the U.S., and make little contribution to the precipitation changes. Stationary wave model results show that neither heating anomalies in the remote tropical Pacific nor those in the nearby Intra-American Sea regions exert much influence on the summertime atmospheric circulation anomalies over the U.S. and nearby regions.

The above results, based on the Scout reanalysis, are supported by two other reanalyses that are available over the period 1948-2004 (the NCEP/NCAR reanalysis and the 20th Century reanalysis). The low-level northeasterly flow anomaly over the southeastern U.S., the key circulation feature that accounts for the U.S. precipitation deficit during fall, as well as the weak and disorganized low-level flow anomaly during summer, is present in all three reanalyses. The relative roles of the diabatic cooling anomalies in the tropical Pacific and those in the Intra-American Sea regions in the maintenance of the northeasterly flow anomaly during fall, nevertheless differs from reanalysis to reanalysis. This suggests considerable uncertainties in the

474 representation of tropical convection. Such uncertainty is not surprising as our composite results
475 are strongly affected by the cold Pacific years during pre-satellite period when these reanalyses
476 lack sufficient observations over tropical oceanic regions and are likely affected by deficiencies
477 in the AGCMs that are used to generate them.

478 The results based on reanalyses suggest that in order to correctly simulate the precipitation
479 response over the U.S. to SST changes in the tropical Pacific, a model must correctly simulate
480 the convection response not only in the tropical Pacific but also in the Intra-American Seas. The
481 NSIPP-1 AGCM appears to be deficient in simulating the warm season tropical convective
482 responses in the Intra-American Seas to the cold Pacific pattern, and consequently the
483 precipitation responses over the U.S. During summer, in contrast to the results based on the
484 Scout reanalysis in which the moderate precipitation deficit over the central U.S. is mainly
485 contributed by reduced local evaporation with little contribution from the rather weak
486 atmospheric circulation anomalies over and to the south of the U.S., the NSIPP-AGCM shows a
487 rather strong and localized precipitation deficit response over the central U.S., and that is
488 balanced roughly equally by a local reduction in evaporation and reduced stationary moisture
489 flux convergences (Wang et al 2010). The above differences in the observationally-based and
490 model-based atmospheric moisture budgets during summer, particularly the contributions of
491 atmospheric circulation changes to U.S. precipitation, originate from the differences in the
492 tropical convection and diabatic heating responses over the Intra-American Sea region.
493 Associated with the cold Pacific SST anomaly, the Scout reanalysis places the enhanced diabatic
494 heating anomaly over the eastern NH tropical Pacific and northern South America which forces
495 rather weak atmospheric circulation anomalies over and to the south of the U.S. (Figure 9a). In
496 comparison, the NSIPP-1 AGCM places the positive heating anomaly over the Gulf of Mexico

(Wang et al 2010, Figure 7) which forces a rather strong low-level cyclonic flow anomaly centered over the Gulf of Mexico that acts to reduce atmospheric moisture transport from the Gulf of Mexico to U.S. land. This type of displacement of the heating response found in the NSIPP-1 AGCM appears to also occur in the other four AGCMs included in the USCLIVAR Drought Working Group project (Schubert et al 2009). In fact, the tropical convection response over the Intra-American Seas to the cold Pacific SST anomaly and the resultant impact over the U.S. precipitation differs considerably from model to model (Wang et al 2010). It remains to be seen if more recent AGCMs have improved performance in this regard.

Acknowledgement:

This study is supported by the NASA Modeling, Analysis and Prediction (MAP) program.

References:

Bacmeister J., P. J. Pegion, S. D. Schubert, and M. J. Suarez, 2000: An atlas of seasonal means simulated by the NSIPP 1 atmospheric GCM. *Vol.* 17. NASA Tech. Memo.104606, Goddard Space Flight Center, Greenbelt, MD, 194 pp.

Compo, G.P., and co-authors, 2011: The Twentieth Century reanalysis Project. *Quarterly J. Roy. Meteorol. Soc*., **137**, 1-28. DOI: 10.1002/qj.776.

Dai, A., 2012: The influence of the Inter-decadal Pacific Oscillation on U.S. precipitation during 1923-2010. Climate Dynamics, DOI 10.1007/s00382-012-1446-5.

Held, I. M., M. Ting, and H. Wang, 2002: Northern winter stationary waves: theory and modeling. *J. Climate*, **15**, 2125-2144.

517 Kalnay, E., and Coauthors, 1996: The NCEP/NCAR 40-Year reanalysis Project. *Bull. Amer.*
518 *Meteor. Soc.*, **77**, 437–471.

519 Koster, R. D., M. J. Suarez, R. W. Higgins, and H. M. van den Dool, 2003: Observational
520 evidence that soil moisture variations affect precipitation. *Geophys. Res. Lett.*, **30,** 1241.
521 doi:10.1029/2002GL016571.

522 Lau N.-C., A. Leetmaa, M.J. Nath, and H-L. Wang, 2005: Influences of ENSO-induced Indo-
523 Western Pacific SST anomalies on extratropical atmospheric variability during the Boreal
524 summer. *J. Climate,* **18**, 2922-2942.

525 Mitchell and Jones, 2005: An improved method of constructing a database of monthly climate
526 observations and associated high-resolution grids. *Int. J. Climatology*, **25**, 693-712, Doi:
527 10.1002/joc.1181.

528 Mo, C. Kingtse, Jae-Kyung E. Schemm, and Soo-Hyun Yoo, 2009: Influence of ENSO and the
529 Atlantic Multidecadal Oscillation on Drought over the United States. *Journal of Climate*, **22**,
530 5962–5982.

531 Pegion, P., S. Schubert, and M. J. Suarez, 2000: An assessment of the predictability of northern
532 winter seasonal means with the NSIPP1 AGCM. *NASA Tech. Memo-2000-104606*, Vol. 18,
533 100pp.

534 Rayner, N. A.; Parker, D. E.; Horton, E. B.; Folland, C. K.; Alexander, L. V.; Rowell, D. P.;
535 Kent, E. C.; Kaplan, A. (2003) Global analyses of sea surface temperature, sea ice, and night

536 marine air temperature since the late nineteenth century J. Geophys. Res.Vol. 108, No. D14,
537 4407 10.1029/2002JD002670.

538 Rienecker, M. M., and Coauthors, 2011: MERRA - NASA's Modern-Era Retrospective Analysis
539 for Research and Applications. *J. Climate*, 24, 3624-3648. doi: 10.1175/JCLI-D-11-00015.1.

540 Schubert S. D., M. J. Suarez, P. J. Pegion, M. A. Kistler, and A. Kumer, 2002: Predictability of
541 zonal means during boreal summer. *J. Climate*, **15**, 420–434.

542 Schubert S. D., M. J. Suarez, P. J. Pegion, R. D. Koster, and J. T. Bacmeister, 2004: Causes of
543 long-term drought in the U.S. Great Plains. *J. Climate*, **17**, 485–503.

544 Schubert Siegfried, and Coauthors, 2009: A U.S. CLIVAR Project to Assess and Compare the
545 Responses of Global Climate Models to Drought-Related SST Forcing Patterns: Overview and
546 Results. *Journal of Climate*, Vol. 22, Iss. 19, pp. 5251–5272.

547 Schubert, Siegfried, Hailan Wang, Max Suarez, 2011: Warm Season Subseasonal Variability and
548 Climate Extremes in the Northern Hemisphere: The Role of Stationary Rossby Waves. *J.*
549 *Climate*, **24**, 4773–4792.

550 Seager, R., Y. Kushnir, C. Herweijer, N. Naik(Henderson) and J. Velez(Nakamura), 2005:
551 Modeling of tropical forcing of persistent droughts and pluvials over western North America:
552 1856-2000. *Journal of Climate*, **18**(19): 4065-4088.

553 Small D. and S. Islam, 2008: Low frequency variability in fall precipitation across the
554 United States, *Water Resour. Res.*, 44, W04426, doi:10.1029/2006WR005623.

555 Small D. and S. Islam, 2009: A synoptic view of trends and decadal variations in autumn
556 precipitation across the United States from 1948 to 2004, *J. Geophys. Res.*, 114, D10102,
557 doi:10.1029/2008JD011579.

558 Small, David, Shafiqul Islam, Mathew Barlow, 2010: The Impact of a Hemispheric Circulation
559 Regime on Fall Precipitation over North America. *J. Hydrometeor*, **11**, 1182–1189.

560 Ting, M. and H. Wang, 1997: Summertime U.S. precipitation variability and its relation to
561 Pacific Sea Surface Temperature. *J. Climate*, **10**,1853-1873.

562 Ting, M. and L. Yu, 1998: Steady response to tropical heating in wavy linear and nonlinear
563 baroclinic models. *J. Atmos. Sci.,* **55**, 3565–3582.

564 Trenberth, K. E., G. W. Branstator, D. Karoly, A. Kumar, N-C. Lau, and C. Ropelewski, 1998:
565 Progress during TOGA in understanding and modeling global teleconnections associated with
566 tropical sea surface temperatures. *J. Geophys. Res.*, **103,** (special TOGA issue), 14291-14324.

567 Wang, Hailan, Mingfang Ting, 1999: Seasonal Cycle of the Climatological Stationary Waves in
568 the NCEP–NCAR reanalysis. *J. Atmos. Sci.*, **56**, 3892–3919.

569 Wang Hailan, Siegfried Schubert, Max Suarez, Randal Koster, 2010: The Physical Mechanisms
570 by which the Leading Patterns of SST Variability Impact U.S. Precipitation. *J. Climate*, **23**, 1815
571 - 1836.

572 Wang Hailan, Siegfried Schubert, Austin Conaty, Meta Sienkiewicz, Douglas Collins, 2010: The
573 post-war (1948-1978) extension of the MERRA Scout. The NASA Global Modeling and

574 Assimilation Office 2009 Annual Research Reports (available at
575 http://gmao.gsfc.nasa.gov/research/reports/GMAO_2009Highlights.pdf), 42-43.

576

577 **List of Figures**

578 Figure 1. The cold Pacific SST pattern (upper panel, unit: K) and its corresponding normalized
579 principal component (lower panel). The cold Pacific SST pattern is obtained as the second
580 leading rotated EOF of the annual mean HadISST v1 over the period of 1901–2004. The
581 amplitude of the cold Pacific pattern reflects two standard deviations of the SST forcing.

582 Figure 2. The observed December-January-February (DJF), March-April-May (MAM), June-
583 July-August (JJA), September-October-November (SON) and annual mean precipitation
584 anomalies (unit: mm/day) over the U.S. associated with the cold Pacific pattern. The
585 observational data is taken from the HadCRU TS3.0 (Mitchell and Jones 2005). The
586 precipitation anomalies are obtained by compositing the HadCRU TS3.0 precipitation using a
587 criteria exceeding one standard deviation of the principal component of the cold Pacific pattern
588 over the period 1901-2004.

589 Figure 3. The DJF, MAM, JJA, SON and annual mean precipitation anomalies (unit: mm/day)
590 over the U.S. associated with the cold Pacific pattern in the Scout reanalysis. The precipitation
591 anomalies are obtained by compositing the Scout reanalysis precipitation using a criteria
592 exceeding one standard deviation of the principal component of the cold Pacific pattern over the
593 period 1948-2004.

Figure 4. Atmospheric moisture budget analysis for (a) DJF, (b) MAM, (c) JJA and (d) SON mean responses to cold Pacific pattern in the Scout reanalysis, based on the data over the period 1948-2004. The responses of precipitation, evaporation, vertically integrated transient moisture flux convergences (Tran), vertically integrated stationary moisture flux convergences due to changes in atmospheric moisture (StatQ), and those due to the changes in atmospheric circulation (StatV) superimposed with the corresponding vertically integrated stationary moisture fluxes are shown. Units: mm day^{-1}.

Figure 5. The SON eddy streamfunction (unit: $m^2\ s^{-1}$) at $\sigma = 0.866$ in (a) the Scout reanalysis; the stationary wave model response to (b) the sum of diabatic heating anomalies and anomalies in transient flux convergences, (c) the diabatic heating anomalies only, (d) anomalies in transient flux convergences, and regional diabatic heating anomalies over (e) west of 250ºE, (f) east of 250ºE, (g) diabatic heating anomaly east of 250ºE, and (h) diabatic cooling anomaly east of 250ºE. The corresponding vertically integrated diabatic heating anomalies (K day^{-1}) are shaded. Contour interval of streamfunction is $0.3 \times 10^6\ m^2\ s^{-1}$ (negative values are dashed and the zero line is the first solid contour).

Figure 6. The JJA eddy streamfunction (unit: $m^2\ s^{-1}$) at $\sigma = 0.866$ in (a) the Scout reanalysis; the stationary wave model response to (b) the sum of diabatic heating anomalies and anomalies in transient flux convergences, (c) the diabatic heating anomalies only, (d) anomalies in transient flux convergences, and regional diabatic heating anomalies over (e) west of 250ºE, and (f) east of 250ºE. The corresponding vertically integrated diabatic heating anomalies (K day^{-1}) are shaded. Contour interval of streamfunction is $0.3 \times 10^6\ m^2\ s^{-1}$ (negative values are dashed and the zero line is the first solid contour).

Figure 7. The JJA and SON mean geopotential height (red contour, unit: m) and wind (blue vector, unit: m/s) anomalies at 850mb associated with the cold Pacific SST pattern in the Scout reanalysis (upper panels), the NCEP/NCAR reanalysis (middle panels), and the 20th Century reanalysis. The anomaly fields are obtained based on composite analysis over the period 1948-2004.

Figure 8. The comparison of JJA (left panels) and SON (right panels) mean precipitation anomalies (unit: mm/day) associated with the cold Pacific pattern between the Scout reanalysis (upper panels), the NCEP/NCAR reanalysis (middle panels), and the 20th Century reanalysis (lower panels).

Figure 9. Left panels: The SON eddy streamfunction (unit: $m^2\ s^{-1}$) at $\sigma = 0.866$ in (a) the NCEP/NCAR reanalysis; the stationary wave model response to the diabatic heating anomalies constructed using the reanalysis precipitation over the (b) global region, (c) west of 250ºE, and (d) east of 250ºE; Right panels show the same as the left panels expect for the 20th Century reanalysis. The corresponding vertically integrated diabatic heating anomalies (K day^{-1}) are shaded. Contour interval of streamfunction is $0.3 \times 10^6\ m^2\ s^{-1}$ (negative values are dashed and the zero line is the first solid contour). The 3-D SON basic states for the two Reanalyses are computed over the period 1948-2004.

Figure 10. Atmospheric moisture budget analysis for (a) DJF, (b) MAM, (c) JJA and (d) SON mean response to cold Pacific pattern in the idealized NASA NSIPP-1 AGCM simulations forced with the cold Pacific SST pattern with SST forcing amplitude corresponding to two standard deviations. The responses of precipitation, evaporation, vertically integrated transient moisture flux convergences (Tran), vertically integrated stationary moisture flux convergences

638 due to changes in atmospheric moisture (StatQ), and those due to the changes in atmospheric
639 circulation (StatV) superimposed with the corresponding vertically integrated stationary moisture
640 fluxes are shown. Note the shading intervals and vector scales are 1.5 times those in Figure 4.
641 Units: mm day^{-1}.

642 Figure 11. The JJA (left panel) and SON (right panel) mean precipitation anomalies (unit: mm
643 day^{-1}) over the U.S. associated with the cold Pacific pattern in the NASA NSIPP-1 AMIP
644 ensemble mean simulations. The precipitation anomalies are obtained by compositing the AMIP
645 ensemble mean precipitation using a criteria exceeding one standard deviation of the PC of the
646 cold Pacific pattern over the period 1948-2004.

647

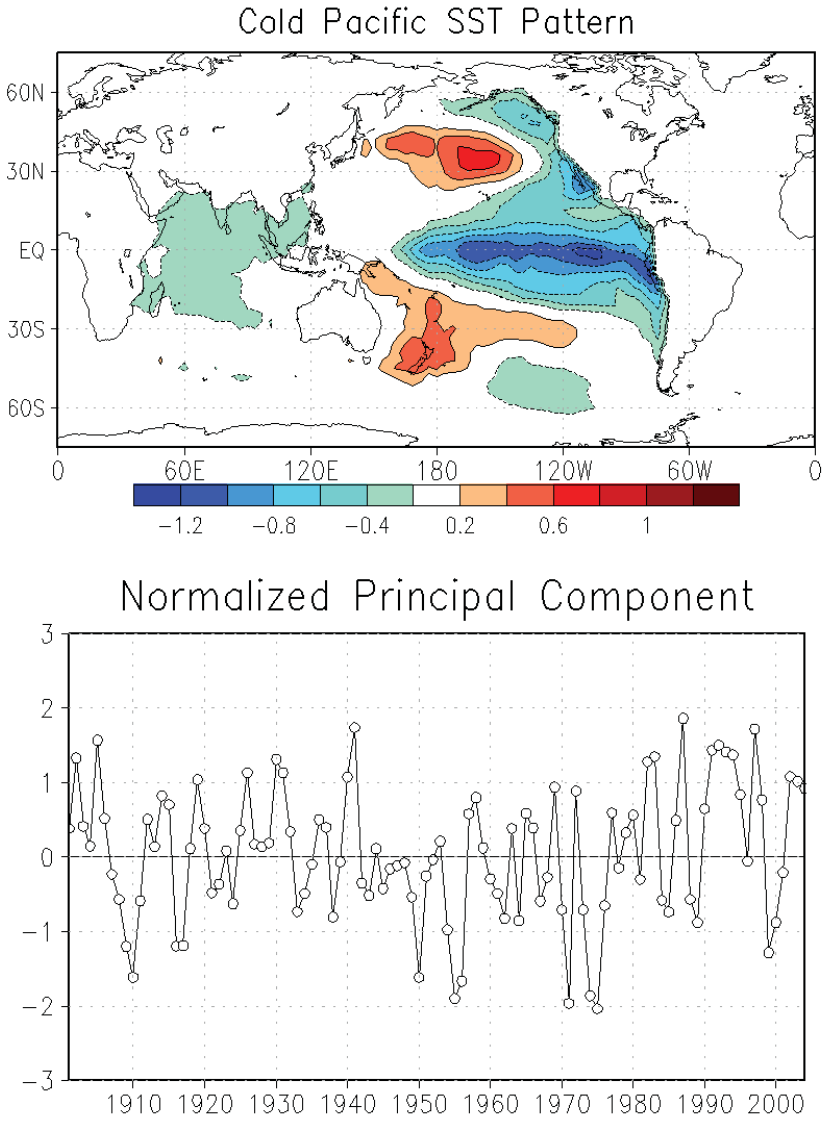

Figure 1. The cold Pacific SST pattern (upper panel, unit: K) and its corresponding normalized principal component (lower panel). The cold Pacific SST pattern is obtained as the second leading rotated EOF of the annual mean HadISST v1 over the period of 1901–2004. The amplitude of the cold Pacific pattern reflects two standard deviations of the SST forcing.

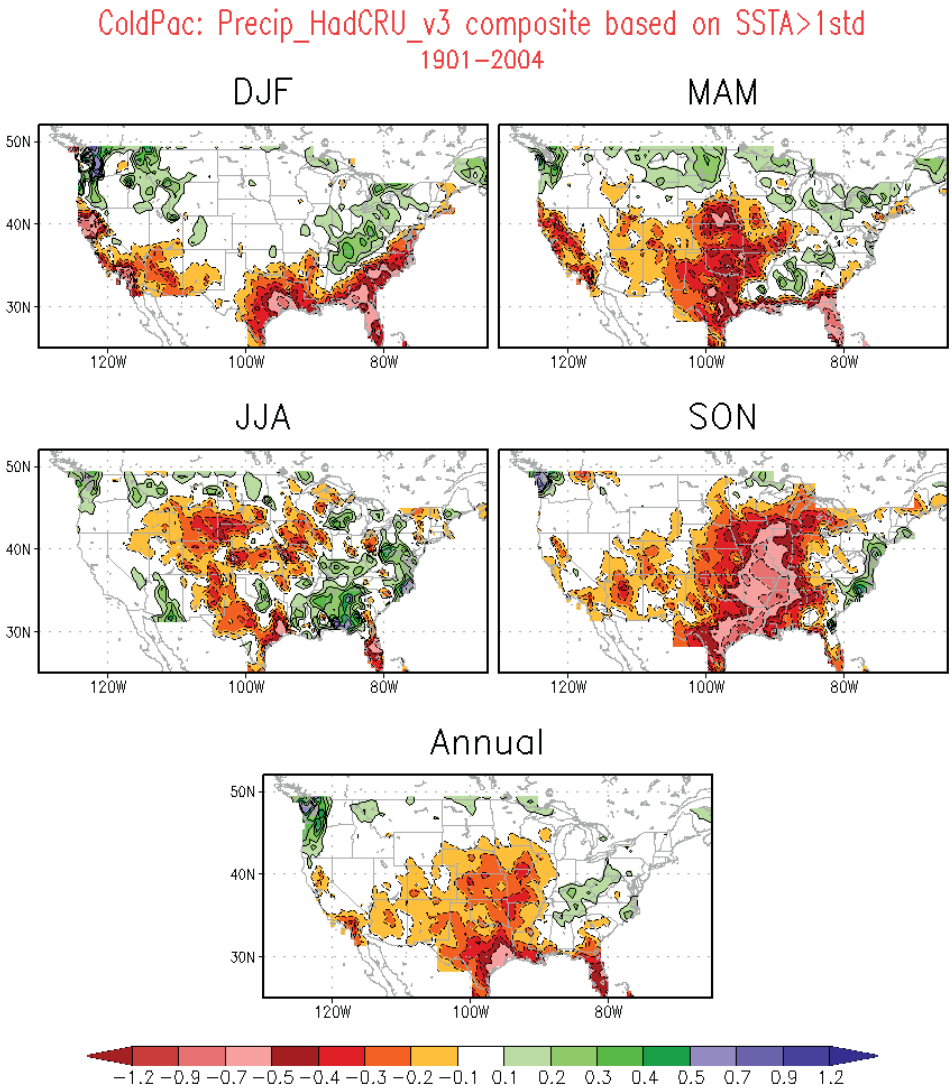

Figure 2. The observed December-January-February (DJF), March-April-May (MAM), June-July-August (JJA), September-October-November (SON) and annual mean precipitation anomalies (unit: mm/day) over the U.S. associated with the cold Pacific pattern. The observational data is taken from the HadCRU TS3.0 (Mitchell and Jones 2005). The precipitation anomalies are obtained by compositing the HadCRU TS3.0 precipitation using a criteria exceeding one standard deviation of the principal component of the cold Pacific pattern over the period 1901-2004.

667

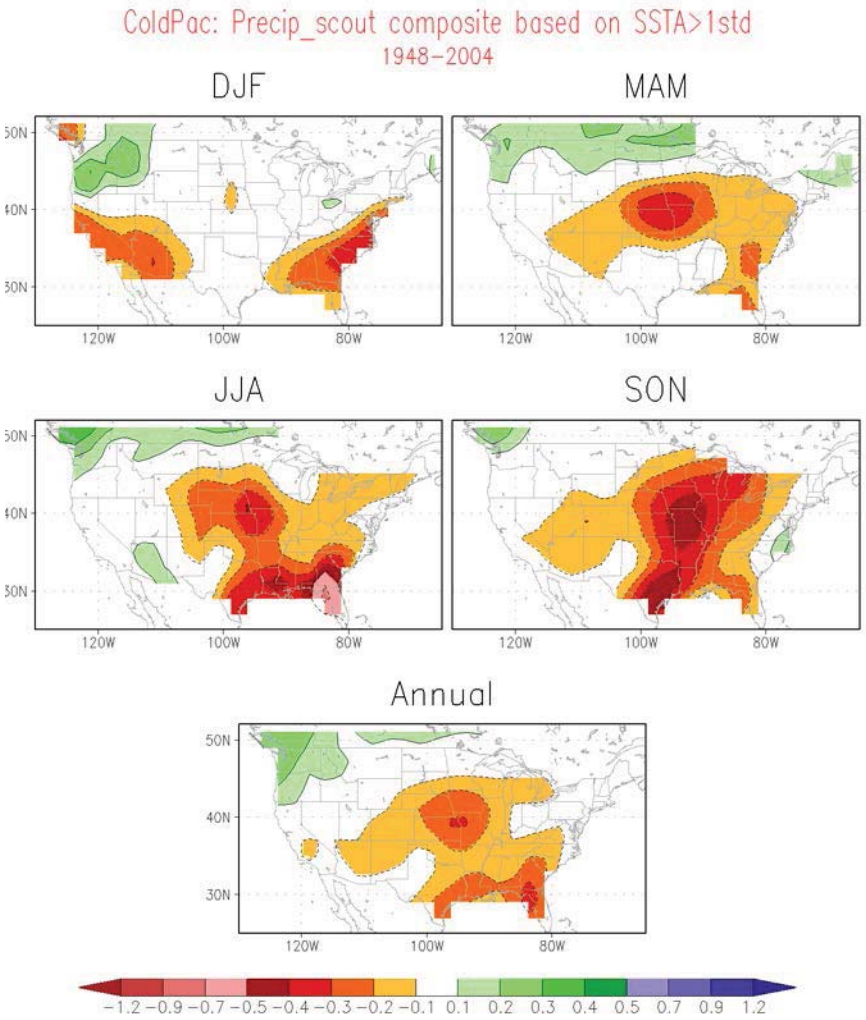

668

669 Figure 3. The DJF, MAM, JJA, SON and annual mean precipitation anomalies (unit: mm/day)
670 over the U.S. associated with the cold Pacific pattern in the Scout reanalysis. The precipitation
671 anomalies are obtained by compositing the Scout reanalysis precipitation using a criteria
672 exceeding one standard deviation of the principal component of the cold Pacific pattern over the
673 period 1948-2004.

674

675

676

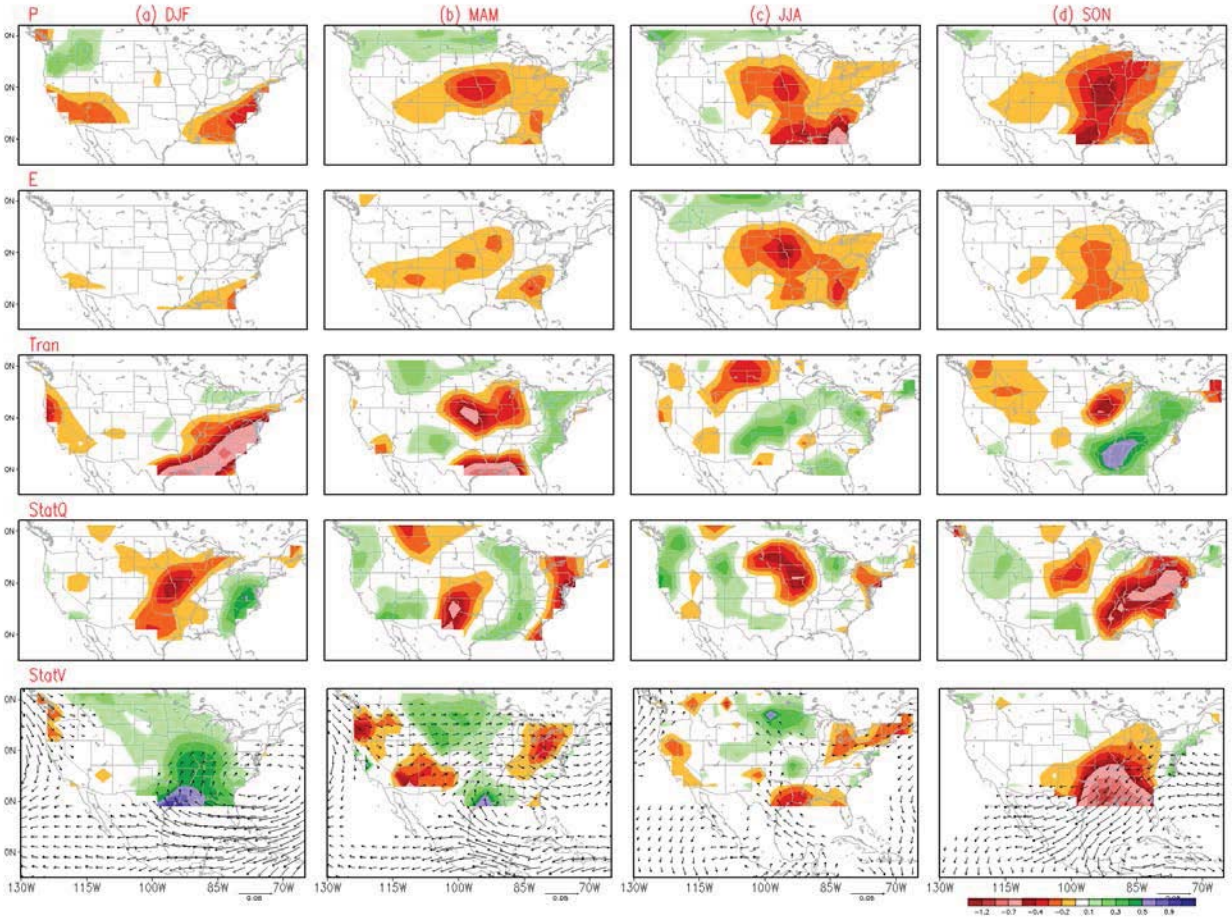

677

678 Figure 4. Atmospheric moisture budget analysis for (a) DJF, (b) MAM, (c) JJA and (d) SON
679 mean responses to cold Pacific pattern in the Scout reanalysis, based on the data over the period
680 1948-2004. The responses of precipitation, evaporation, vertically integrated transient moisture
681 flux convergences (Tran), vertically integrated stationary moisture flux convergences due to
682 changes in atmospheric moisture (StatQ), and those due to the changes in atmospheric circulation
683 (StatV) superimposed with the corresponding vertically integrated stationary moisture fluxes are
684 shown. Units: mm day^{-1}.

685

686

687

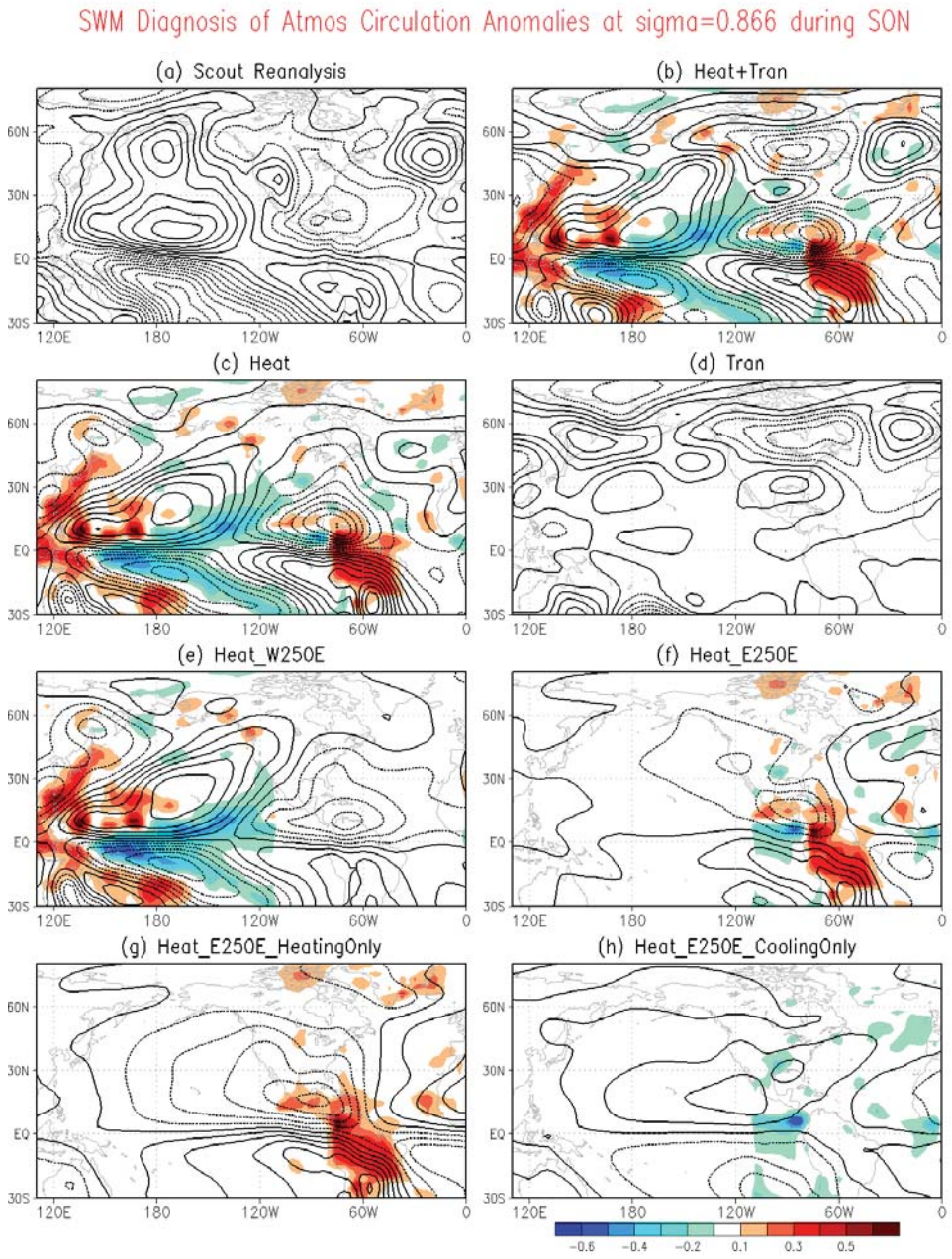

688

689 Figure 5. The SON eddy streamfunction (unit: $m^2\ s^{-1}$) at $\sigma = 0.866$ in (a) the Scout reanalysis; the
690 stationary wave model response to (b) the sum of diabatic heating anomalies and anomalies in
691 transient flux convergences, (c) the diabatic heating anomalies only, (d) anomalies in transient
692 flux convergences, and regional diabatic heating anomalies over (e) west of 250ºE, (f) east of
693 250ºE, (g) diabatic heating anomaly east of 250ºE, and (h) diabatic cooling anomaly east of
694 250ºE. The corresponding vertically integrated diabatic heating anomalies (K day^{-1}) are shaded.

Contour interval of streamfunction is 0.3×10^6 m^2 s^{-1} (negative values are dashed and the zero line is the first solid contour).

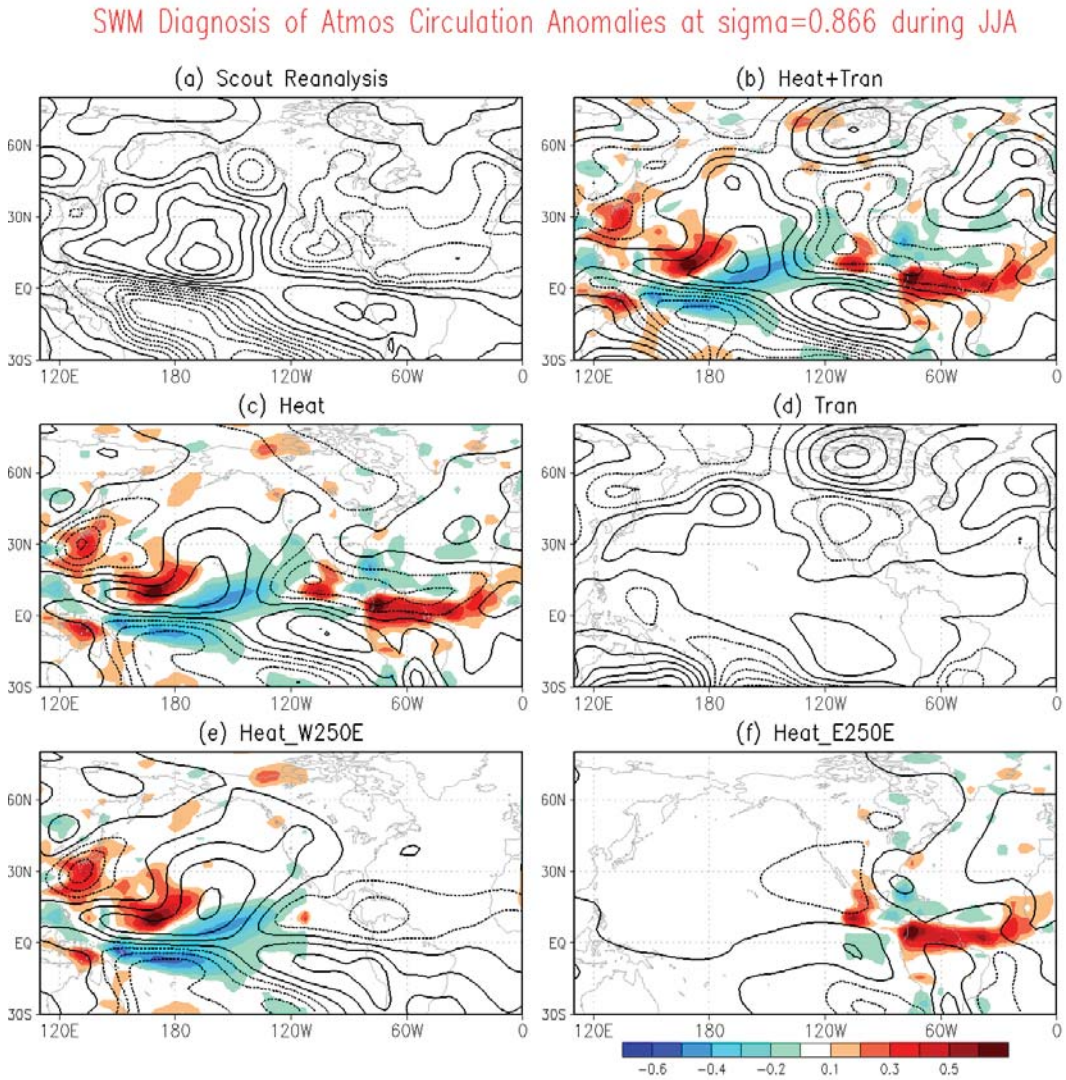

Figure 6. The JJA eddy streamfunction (unit: m^2 s^{-1}) at $\sigma = 0.866$ in (a) the Scout reanalysis; the stationary wave model response to (b) the sum of diabatic heating anomalies and anomalies in transient flux convergences, (c) the diabatic heating anomalies only, (d) anomalies in transient flux convergences, and regional diabatic heating anomalies over (e) west of 250ºE, and (f) east of 250ºE. The corresponding vertically integrated diabatic heating anomalies (K day^{-1}) are shaded. Contour interval of streamfunction is 0.3×10^6 m^2 s^{-1} (negative values are dashed and the zero line is the first solid contour).

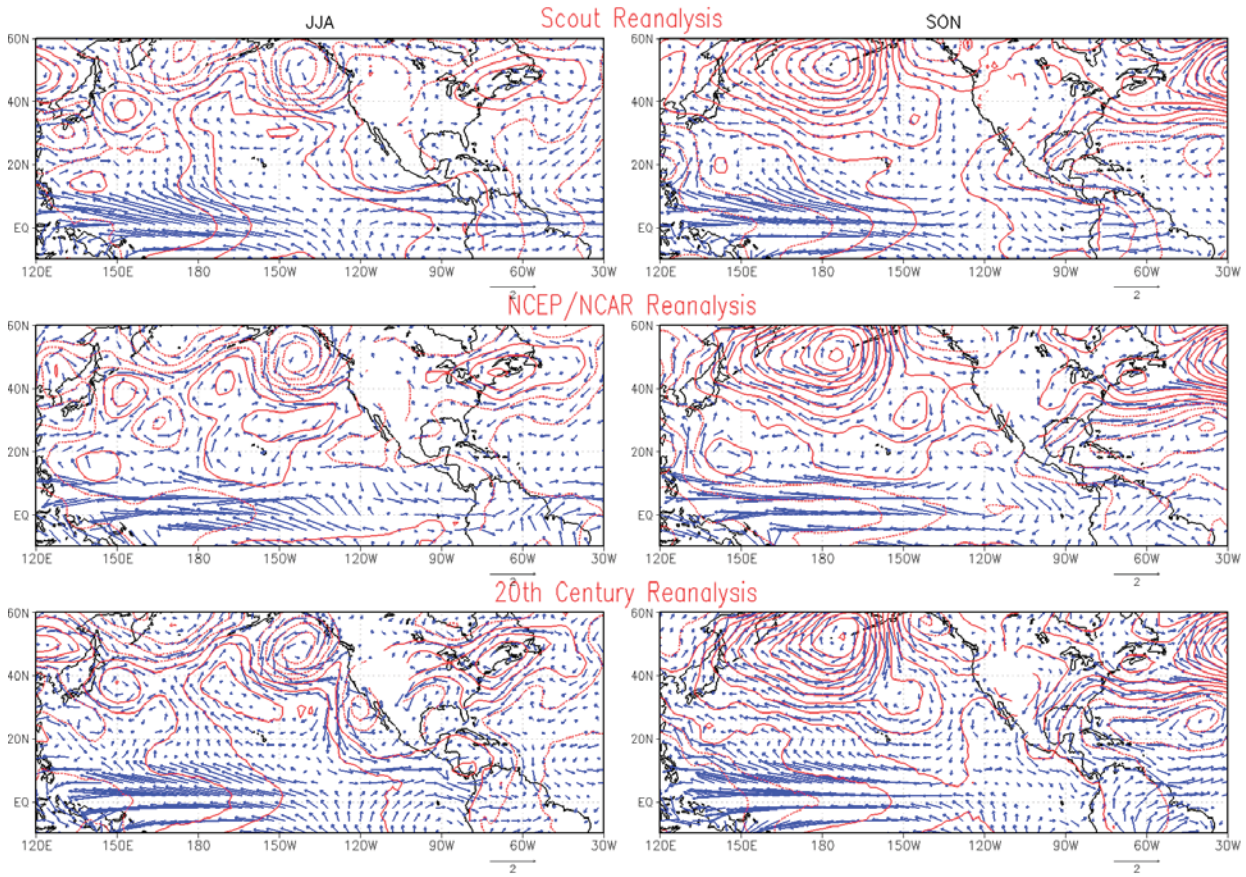

Figure 7. The JJA and SON mean geopotential height (red contour, unit: m) and wind (blue vector, unit: m/s) anomalies at 850mb associated with the cold Pacific SST pattern in the Scout reanalysis (upper panels), the NCEP/NCAR reanalysis (middle panels), and the 20th Century reanalysis. The anomaly fields are obtained based on composite analysis over the period 1948-2004.

716

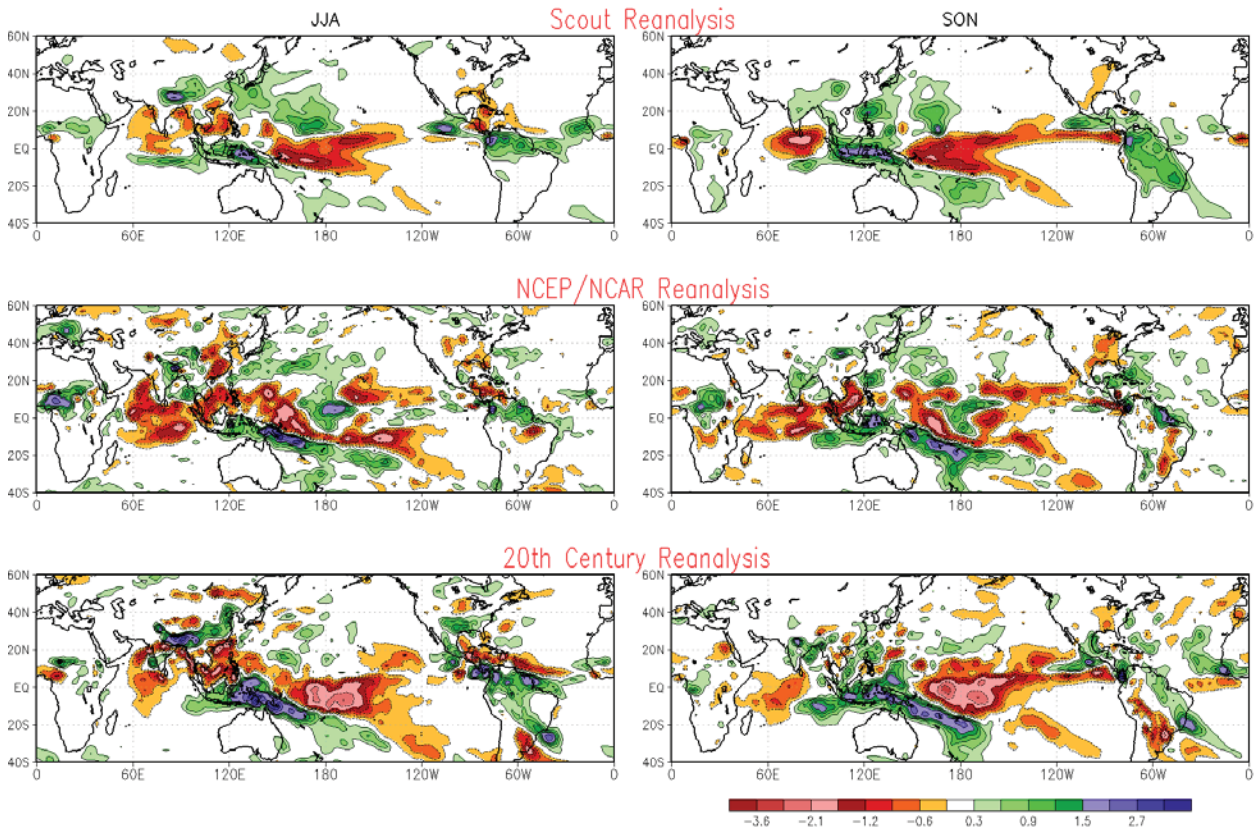

717

718 Figure 8. The comparison of JJA (left panels) and SON (right panels) mean precipitation
719 anomalies (unit: mm/day) associated with the cold Pacific pattern between the Scout reanalysis
720 (upper panels), the NCEP/NCAR reanalysis (middle panels), and the 20th Century reanalysis
721 (lower panels).

722

723

724

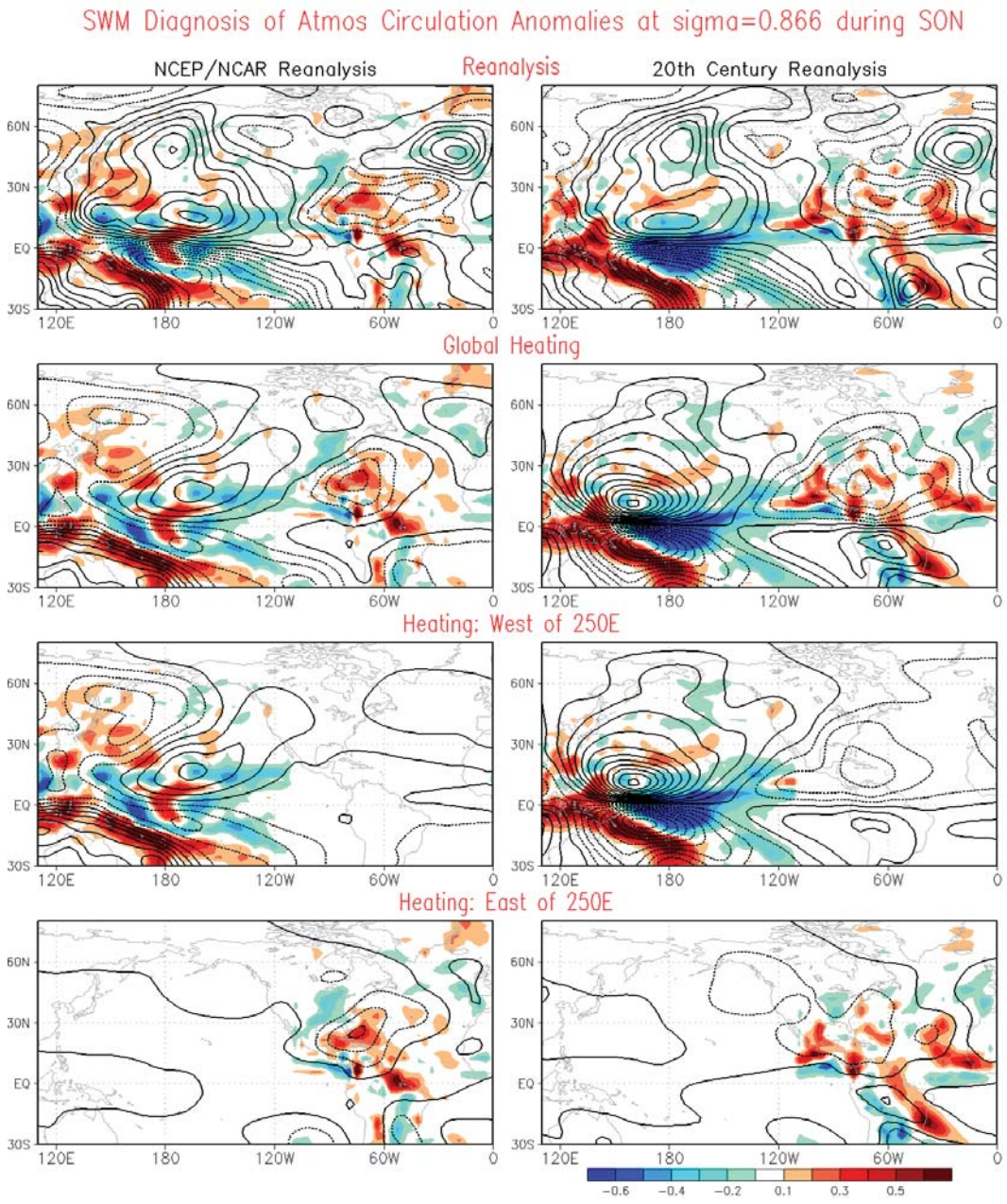

725

726 Figure 9. Left panels: The SON eddy streamfunction (unit: $m^2\ s^{-1}$) at $\sigma = 0.866$ in (a) the
727 NCEP/NCAR reanalysis; the stationary wave model response to the diabatic heating anomalies
728 constructed using the reanalysis precipitation over the (b) global region, (c) west of 250ºE, and
729 (d) east of 250ºE; Right panels show the same as the left panels expect for the 20th Century
730 reanalysis. The corresponding vertically integrated diabatic heating anomalies (K day^{-1}) are
731 shaded. Contour interval of streamfunction is $0.3 \times 10^6\ m^2\ s^{-1}$ (negative values are dashed and
732 the zero line is the first solid contour). The 3-D SON basic states for the two Reanalyses are
733 computed over the period 1948-2004.

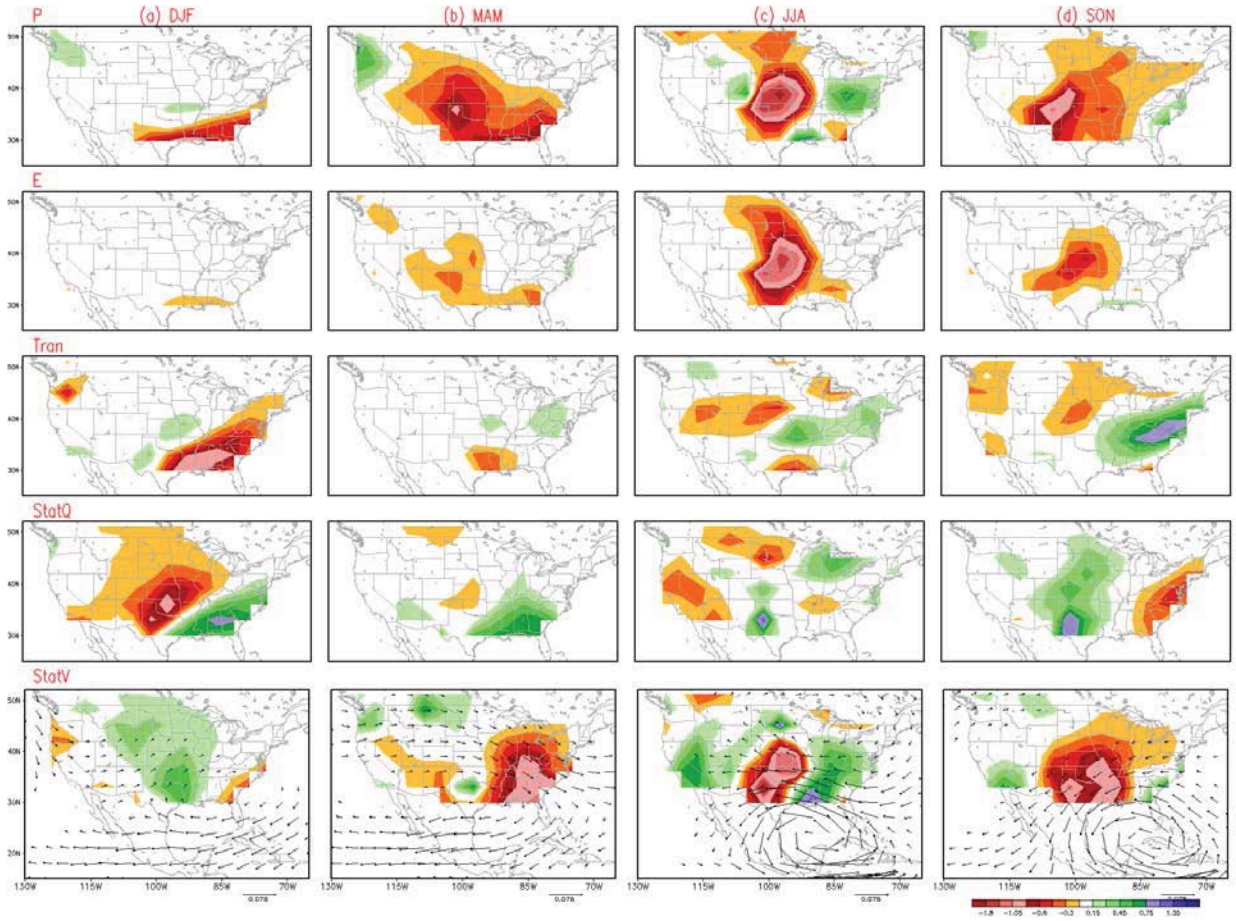

Figure 10. Atmospheric moisture budget analysis for (a) DJF, (b) MAM, (c) JJA and (d) SON mean response to cold Pacific pattern in the idealized NASA NSIPP-1 AGCM simulations forced with the cold Pacific SST pattern with SST forcing amplitude corresponding to two standard deviations. The responses of precipitation, evaporation, vertically integrated transient moisture flux convergences (Tran), vertically integrated stationary moisture flux convergences due to changes in atmospheric moisture (StatQ), and those due to the changes in atmospheric circulation (StatV) superimposed with the corresponding vertically integrated stationary moisture fluxes are shown. Note the shading intervals and vector scales are 1.5 times those in Figure 4. Units: mm day^{-1}.

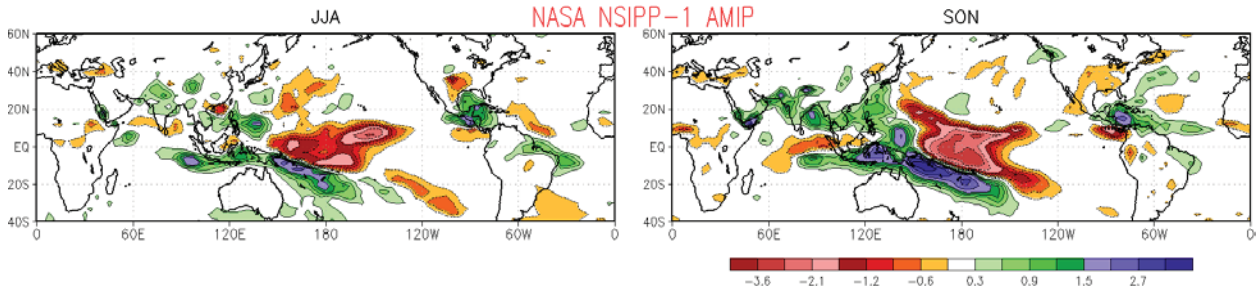

748

749 Figure 11. The JJA (left panel) and SON (right panel) mean precipitation anomalies (unit: mm
750 day^{-1}) over the U.S. associated with the cold Pacific pattern in the NASA NSIPP-1 AMIP
751 ensemble mean simulations. The precipitation anomalies are obtained by compositing the AMIP
752 ensemble mean precipitation using a criteria exceeding one standard deviation of the PC of the
753 cold Pacific pattern over the period 1948-2004.

754

755